scientific reports

Check for updates

OPEN

Structural and biomedical investigations of novel ruthenium schiff base complexes

Ramadan M. Ramadan, Hadeel H. El-Shalakany & Mostafa A. Sayed✉

Ruthenium(III) complexes with Schiff base ligands bearing diverse functional groups remain extensively underexplored, despite their promising potential in therapeutic applications. To address this gap, we designed and synthesized a new series of mononuclear octahedral Ru(III) complexes with the general formula [RuL$^{1-3}$], where L^1, L^2, and L^3 are deprotonated Schiff bases derived from functionalized aromatic precursors. These complexes were characterized through a suite of physicochemical and spectroscopic techniques, including FT-IR, ^{1}H-NMR, UV-Vis spectroscopy, mass spectrometry, TGA, and elemental analysis, to confirm their structural features and coordination environment. To complement experimental findings, density functional theory (DFT/B3LYP) calculations were conducted, revealing stable, distorted octahedral geometries and supporting the proposed molecular configurations. Building upon the structural insights, we evaluated the biological activity of the complexes through in vitro cytotoxicity assays against HCT-116 (colorectal), MCF-7 (breast), and HepG2 (liver) cancer cell lines. Among them, RuL^2 exhibited the most potent activity against HCT-116 (IC_{50} = 4.97 µg/mL), comparable to the standard drug Vinblastine. Finally, molecular docking simulations were employed to investigate the interaction of these complexes with key biological targets from *Escherichia coli* (PDB IDs: 4BJP and 1BNA), offering further insights into their potential modes of action. Together, these results demonstrate the importance of ligand design in tuning the coordination behavior and bioactivity of ruthenium complexes, highlighting their promise in anticancer and antimicrobial drug development.

Keywords Ru(III) complexes, Schiff base ligands, Molecular docking, DFT analysis, Biological activity

Schiff bases, characterized by the imine (-C = N-) functional group, are widely utilized in coordination chemistry due to their ability to form stable and structurally diverse metal complexes[1–3]. Typically synthesized through the condensation of primary amines with carbonyl compounds, Schiff bases offer versatile donor atoms—commonly nitrogen (N), oxygen (O), and sulfur (S)—that promote strong chelation with metal centers[4–7]. The nature and arrangement of these donor atoms significantly influence the geometry, stability, and reactivity of the resulting complexes, as well as their interaction with biological targets such as DNA and proteins[8–12]. Incorporation of electron-donating (e.g., hydroxyl, methoxy) or electron-withdrawing (e.g., nitro, chloro) substituents into the Schiff base framework further tunes the electronic properties of metal complexes, impacting their redox behavior, lipophilicity, and biological activity[13–15]. Owing to these tunable features, Schiff base complexes have demonstrated a wide spectrum of pharmacological properties, including antibacterial, antifungal, antioxidant, antidiabetic, and anticancer effects[16–18]. Furthermore, the biological function of Schiff base metal complexes is strongly influenced by the specific donor atoms present and their three-dimensional configuration[19,20].

Cancer remains a leading cause of mortality worldwide, and current chemotherapeutic agents, especially platinum-based drugs such as cisplatin, are associated with severe side effects and the emergence of drug resistance[21]. These limitations necessitate the search for new metal-based therapeutics with enhanced selectivity and lower toxicity. Ruthenium complexes have emerged as promising candidates due to their favorable pharmacokinetics, redox versatility, and ability to engage in multiple modes of action, including DNA binding and protein inhibition[22–25]. Compared to platinum-based medications, ruthenium complexes have demonstrated remarkable antitumor activity, along with improved efficacy, reduced drug resistance, and less toxicity[26]. Ruthenium complexes incorporating Schiff base ligands have shown remarkable potential in biological applications, notably in antioxidant, antimicrobial, and anticancer activities[27,28]. The octahedral coordination geometry favored by both Ru(II)/Ru(III) is a key factor in the effectiveness of these ruthenium complexes[29].

Chemistry Department, Faculty of Science, Ain Shams University, Cairo 11566, Egypt. ✉email: mostafa_abdellah@sci.asu.edu.eg

Particularly, ruthenium(III) complexes with Schiff base ligands have shown potent cytotoxicity against various cancer cell lines and notable antimicrobial activity[30,31].

The biological performance of these complexes is highly dependent on the structural and electronic characteristics of the ligand. Functional groups such as hydroxyl, methoxy, and nitro have been reported to enhance DNA-binding affinity, cellular uptake, and selective toxicity toward cancer cells[32]. Moreover, Schiff base ligands significantly influence the spatial configuration and redox behavior of ruthenium centers, thus affecting their biological mechanisms of action[33,34]. Previous studies have shown that Schiff base Ru(III) complexes exhibit notable cytotoxicity against various cancer cell lines, with IC_{50} values often comparable to or better than standard drugs[24,35–38]. Despite the therapeutic potential of ruthenium(III) complexes, their coordination chemistry and biomedical applications remain underexplored, particularly with Schiff base ligands bearing diverse functional groups.

In this study, we report on the synthesis and comprehensive investigation of three novel mononuclear ruthenium(III) complexes bearing Schiff base ligands HL^1, HL^2, and H_2L^3. These ligands were strategically selected for their distinct functional groups—nitro, chloro, methoxy, and hydroxyl—which are known to influence both coordination behavior and bioactivity. The study encompasses physicochemical characterization, DFT-based structural modeling, and evaluation of anticancer and antimicrobial properties. Cytotoxic effects were assessed against HepG2 (liver), MCF-7 (breast), and HCT-116 (colon) cancer cell lines, while molecular docking studies provided further insight into the complexes' interactions with biomolecular targets. This work aims to elucidate the structure–activity relationships of ruthenium Schiff base complexes and contribute to the development of new metal-based agents in medicinal inorganic chemistry.

Experimental

Materials

$RuCl_3$, 2-amino-3-hydroxypyridine, 2-chloro-5-nitrobenzaldehyde, 2-hydroxy-3-methoxybenzaldehyde and 2-amino-4,6-dimethylpyrimidine were obtained from Sigma-Aldrich.

The physicochemical measurements

Fourier transform infrared (FT-IR) spectra were collected using a Shimadzu FT-IR model 8101 spectrophotometer, with KBr pellets, over the wavelength range of 4000 to 400 cm^{-1}. The conductivity of the ruthenium complexes was measured in 1×10^{-3} M solutions of DMF at room temperature using a JENWAY 4320 conductivity meter. The UV-vis spectra of the ligands and their complexes (1×10^{-5} M) were performed by using a Shimadzu 1800 UV-Vis spectrophotometer. All synthesized compounds underwent elemental analysis (C, H, N) using a PerkinElmer-2400 CHN analyzer to determine their elemental composition. This analysis served as a crucial step in validating the accuracy of the proposed molecular formula for each synthesized compound. A Bruker apparatus (Munich, Germany) was used to carry out the proton nuclear magnetic resonance (^{1}H-NMR) measurements using DMSO-*d6*. Mass spectra were executed using the EI technique at 70 eV via MS-5988 GC-MS Hewlett-Packard equipment. A Shimadzu Corporation 60 H analyzer was used for the thermogravimetric (TG) measurements. The samples were heated in air at a constant heating rate of 10 °C per minute until a maximum temperature of 1000 °C was achieved.

Syntheses

Synthesis of Imine schiff base ligands

Syntheses of the Schiff bases ($\mathbf{HL^1}$ = 2-((2-chloro-5-nitrobenzylidene)amino)pyridin-3-ol, $\mathbf{HL^2}$ = 2-(((4,6-dimethylpyrimidin-2-yl)imino)methyl)-6-methoxyphenol and $\mathbf{H_2L^3}$ = 2-((2-hydroxy-3-methoxybenzylidene)amino)pyridin-3-ol) were carried out by condensing equimolar amounts of either 2-amino-3-hydroxypyridine or 2-amino-4,6-dimethylpyrimidine with either 2-chloro-5-nitrobenzaldehyde or 2-hydroxy-3-methoxybenzaldehyde in absolute ethanol for 2 h. The purity and follow up of the formed ligands were identified using thin layer chromatography (TLC). The resulting imine residues were filtered, recrystallized from hot ethanol, and then kept dry. The synthetic process for the Schiff base ligands is depicted in Fig. 1.

Synthesis of the ruthenium(III) complexes

The ruthenium complexes were synthesized by dissolving equimolar amounts (1 mmol) of $RuCl_3$ and the respective Schiff base ligand in ethanol, followed by refluxing the mixture under stirring for approximately 5 h. After cooling, the solvent was removed, and the resulting solid was purified by washing with hot petroleum ether and recrystallizing from hot ethanol. Figure 2 visually depicts this synthesis and the proposed molecular structures of the ruthenium complexes.

DFT analysis

Gaussian 09 W software was utilized to conduct DFT/B3LYP computations for the purpose of determining the energetically optimized geometries of complexes[39]. The LANL2DZ basis set was employed for the ruthenium complexes. Additional experimental details are provided in the Supplementary Information.

Molecular docking study

The molecular docking analyses were carried out using the Molecular Operating Environment (MOE) program (2014.0901). Two macromolecular biological targets, a penicillin-binding protein 3 from *Escherichia Coli* (PDB ID: 4BJP)[40] and a B-DNA (PDB ID: 1BNA)[41] were screened. The PDB files of the targets were obtained from the Research Collaboratory for Structural Bioinformatics (RCSB) database. Preparation of the macromolecular target involved a sequence of actions: removing solvent molecules from the cavity, stabilizing charges, filling

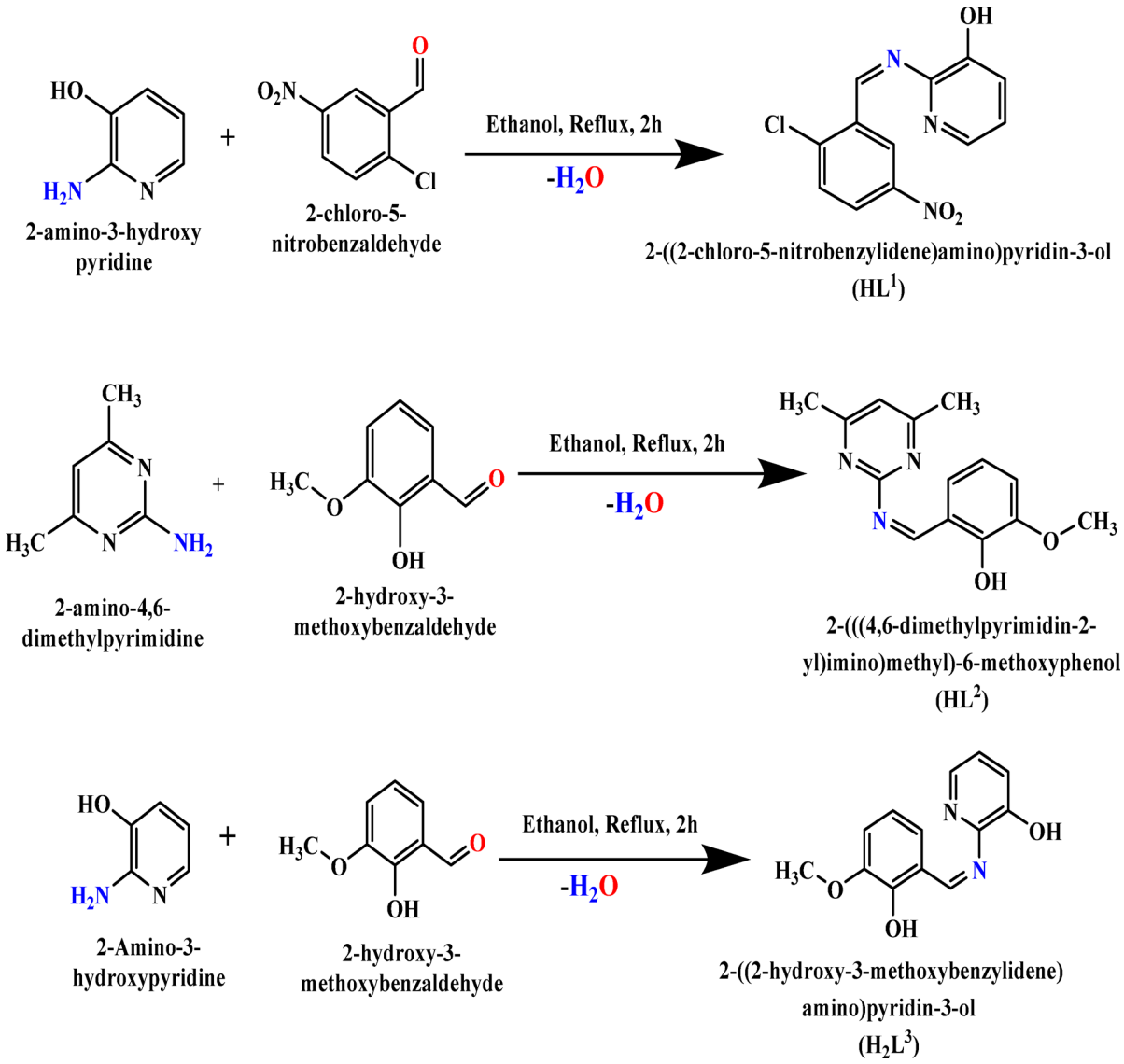

Fig. 1. The synthetic pathways for the studied Schiff base ligands (**HL**^{1}, **HL**^{2} and **H$_2$L**^{3}).

missing residues and hydrogens, optimizing the structure, and fixing the potential. The assembly of the docked ligand was drawn in Chemdraw format, inserted into the MOE main page and then carried out structure optimization.

Biomedical investigations

The antibacterial potency of the ruthenium complexes against *Escherichia coli*, *Serratia marcescens* (Gram-negative), and *Micrococcus luteus* (Gram-positive) was determined using the paper disc diffusion method[42]. The in vitro antitumor screening tests were conducted using three human cancer cell lines: MCF-7 (breast cancer), HCT-116 (colon carcinoma), and HepG2 (liver carcinoma). The cell lines were procured from the VACSERA Tissue Culture Unit, located in Dokki, Giza, Egypt. Detailed experimental procedures are provided in the Supplementary Information.

Results and discussion

Three mononuclear Ru(III) complexes with bi- and tridentate Schiff base ligands having NO-, NNO- and NOO donor atoms, namely, 2-((2-chloro-5-nitrobenzylidene)amino)pyridin-3-ol (**HL**^{1}), 2-(((4,6-dimethylpyrimidin-2-yl)imino)methyl)-6-methoxyphenol (**HL**^{2}), and 2-((2-hydroxy-3-methoxybenzylidene)amino)pyridin-3-ol (**H$_2$L**^{3}) were synthesized and fully characterized by various analytical and spectroscopic techniques. The Ru-complexes were found to be neutral and have unique intense color and air stability. They were insoluble in most organic solvents except for DMF and DMSO. The molar conductivities (Λm) of 1×10^{-3} M DMF solutions of the Ru-complexes ranged between 1.1 and 1.82 $\Omega^{-1}mol^{-1}cm^2$ at 25 °C. These low values reflected the non-electrolytic characteristics of the reported complexes[5]. In addition, the magnetic measurements for the Ru(III), d^5, complexes

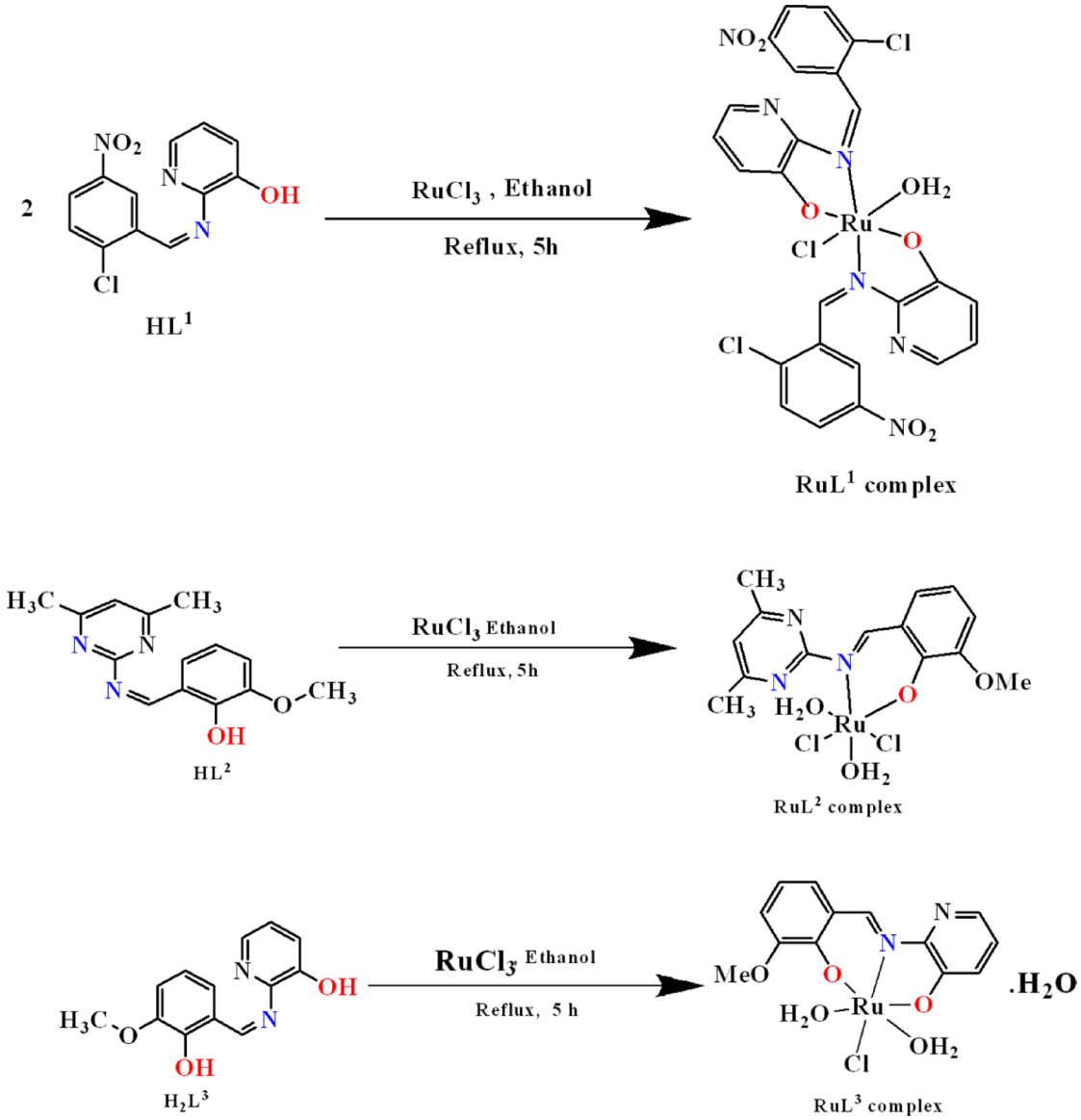

Fig. 2. A schematic representation of the synthetic procedures and the proposed structures of ruthenium(III) complexes.

showed that the values of effective magnetic moments (μ_{eff}) were slightly lower than the spin-only value for one unpaired electron (1.45–1.59 BM). The observed magnetic moments were consistent with the postulated octahedral geometry with low-spin electronic configuration. Mass spectrometry analyses were performed for the ligands and complexes to verify the chemical and molecular structures of the new compounds. The mass spectra of the Schiff base ligands displayed prominent ion peaks at 277, 257, and 246, which corresponded to the parent molecular ions of the formulas $[C_{12}H_8N_3O_3Cl]^+$, $[C_{14}H_{15}N_3O_2]^+$, and $[C_{13}H_{12}N_2O_3+2H]^+$, respectively (Fig. 3). Furthermore, the mass spectrometry results for the ruthenium complexes closely matched the values obtained from elemental analyses, as depicted in Fig. 4. The mass spectrum of **RuL^1** complex demonstrated a remarkable peak at 706.3, which aligns perfectly with the molecular ion $[C_{24}H_{16}N_6O_7Cl_3Ru\text{-}H]^+$. The mass spectrum of the **RuL^2** complex also exhibited the molecular ion peak at 443.7 corresponding to $[C_{14}H_{16}N_3O_3Cl_2Ru\text{-}H_2]^+$. In addition, the EI-mass spectrum of **RuL^3** complex showed molecular ion peak at 414.4 corresponding to $[C_{13}H_{16}N_2O_6ClRu\text{-}H_2O]^+$. Following and tracking the different fragments in the mass spectra of the reported compounds shed more insight into the structure of them. For example, the mass spectrum of **HL^1** ligand displayed fragments at m/z = 260 and 242 due to $[P\text{-}OH]^+$ and $[P\text{-}HCl]^+$, respectively. In addition, the mass spectrum of **HL^2** ligand exhibited the fragments $[P\text{-}C_2H_6]^+$ and $[P\text{-}(OH+C_2H_6)]^+$ at m/z = 228 and 214, respectively. For the **H_2L^3** ligand, the mass spectrum showed three fragments at m/z equal to 228, 213 and 149 corresponding to the fragments [P-OH[$^+$, [P-2OH[$^+$ and $[P\text{-(py-OH)}]^+$, respectively. On the other hand, the mass spectra of the the three ruthenium complexes displayed fragments that confirm their molecular structures. For instance, the **RuL^1** complex showed fragments at m/z = 673, 610 and 567 due to the fragments $[P\text{-Cl}]^+$, $[P\text{-}(H_2O+Cl+NO_2)]^+$ and $[P\text{-}(H_2O+2Cl+NO_2)]^+$, respectively. The mass spectrum of the **RuL^2**, on the other side, displayed the three

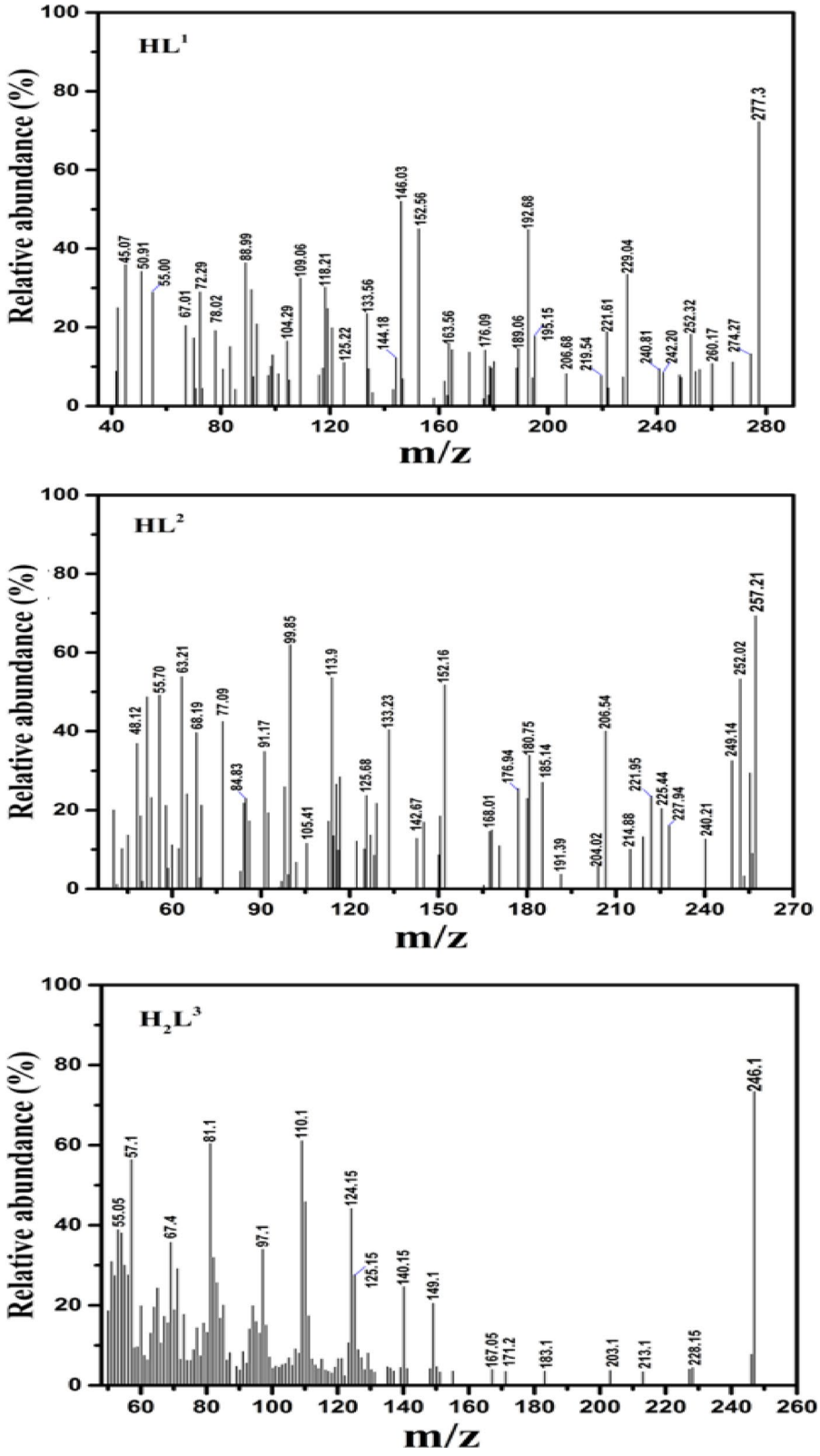

Fig. 3. The mass spectra of the Schiff base ligands.

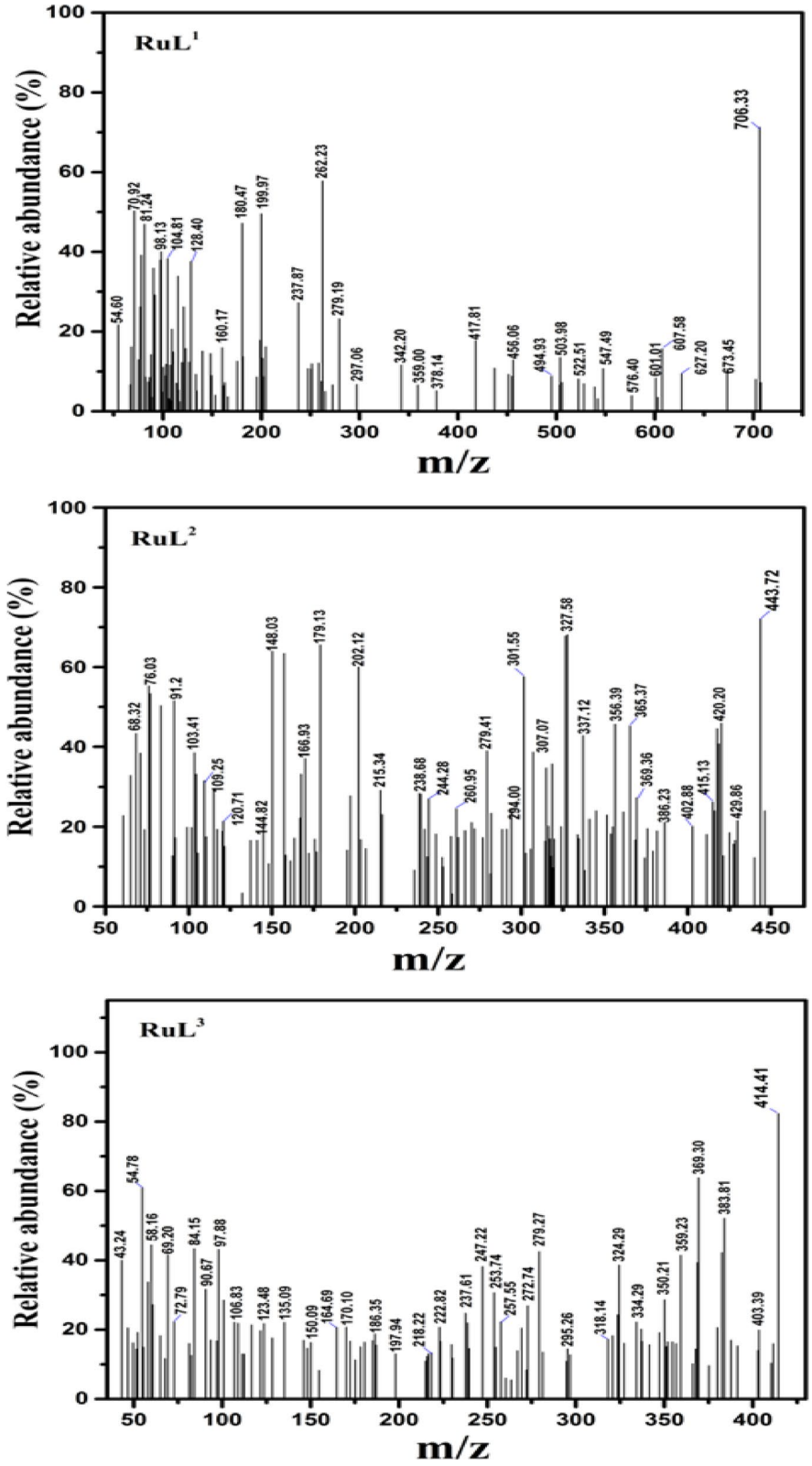

Fig. 4. The mass spectra of the developed Ru(III) complexes.

Compound	Color	Empirical formula	M.wt. (g/mol)	m/z (EI-Mass)	M.P (°C)	Found (Calculated)			Λ_m ($cm^2\ \Omega^{-1}\ mol^{-1}$)
						%C	%H	%N	
HL[1]	Dark brown	$C_{12}H_8N_3O_3Cl$	277.66	277.3	>300	50.66 (51.86)	2.93 (2.88)	14.79 (15.12)	–
HL[2]	Orange	$C_{14}H_{15}N_3O_2$	257.28	257.2	70	65.06 (65.29)	5.28 (5.83)	13.1 (16.32)	–
H_2L^3	Red	$C_{13}H_{12}N_2O_3$	244.24	246.1	250	62.5 (63.87)	4.73 (4.91)	11.83 (11.46)	–
RuL[1]	Black	$C_{24}H_{16}N_6O_7Cl_3Ru$	707.89	706.3	>300	41.39 (40.68)	3.28 (2.26)	12.51 (11.87)	1.1
RuL[2]	Greenish black	$C_{14}H_{18}N_3O_4Cl_2Ru$	464.29	443.7	170	37.32 (36.22)	4.09 (3.91)	10.95 (9.05)	1.82
RuL[3]	Black	$C_{13}H_{16}N_2O_6ClRu$	432.79	414.4	>300	35.88 (36.04)	3.4 (3.7)	7.33 (6.47)	1.63

Table 1. The microanalyses and physicochemical data for the synthesized compounds.

Compound*	$\upsilon(OH)_L$	$\upsilon(OH)_W$	δ(OH)	υ(C=*N*)	$\upsilon(C\text{-}O)_{phenolic}$	υ(M-O)	υ(M-*N*)
HL[1]	3386	–	1490	1613	1345	-	–
HL[2]	3396	–	1460	1590	1384	-	–
H_2L^3	3444	–	1464	1619	1304	-	–
RuL[1]	–	3375	1495	1614	1346	526	467
RuL[2]	–	3419	1478	1602	1367	507	439
RuL[3]	–	3375	1462	1641	1318.	536	446

Table 2. FT-IR spectral data for the ligands and their ruthenium complexes. * *L* ligand, *W* water.

Compound	$(\text{-}OH)_{phenolic}$	HC=*N*	$\text{-}OCH_3$	Aromatic protons
HL[1]	10.33 (s)	8.53 (s)	–	6.42–7.99 (m)
HL[2]	10.26 (s)	10.21(s)	3.84 (s)	6.29–7.25(m)
H_2L^3	10.25 (s)	9.42 (s)	3.81 (s)	6.39–7.41 (m)

Table 3. The ^{1}H-NMR spectral data (δ, ppm) of the schiff base ligands.

fragments $[P\text{-}H_2O]^+$, $[P\text{-}(H_2O+2Cl)]^+$ and $[P\text{-}(H_2O+Cl+C_2H_6)]^+$, at m/z = 429, 357 and 365, respectively. Furthermore, the mass spectrum of the **RuL[3]** complex showed the following fragments: $[P\text{-}MeOH]^+$ (384), $[P\text{-}(H_2O+Cl)]^+$ (360), $[P\text{-}(2H_2O+MeOH)]^+$ (348) and $[P\text{-}(2H_2O+Cl)]^+$ (343). Microanalytical and relevant physicochemical data for the synthesized Schiff base ligands and their complexes are comprehensively summarized in Table 1.

FT-IR and ^{1}H-NMR investigations

Comparison of the FT-IR spectra of the free Schiff base ligands (Figs. 1 and 2 S) with those of their Ru(III)-complexes (Figs. 4 and 5 S) was conducted to examine the electronic structure and the binding interactions between the ligands and the ruthenium(III) ion in the complex sphere. Table 2 displays the IR data of ligands and their corresponding complexes. Schiff bases can form coordination bonds with metal ions through their azomethine and phenolic functional groups. The free ligands exhibited broad vibrational stretching frequency bands at 3386, 3396 and 3444 cm^{-1} due to hydroxyl group of the phenolic part of ligands. The observed intensity and spectral range of the υ(OH) band indicated the presence of intramolecular hydrogen bonding between the OH proton and the neighboring azomethine nitrogen[43–45]. It is noteworthy that all of the complexes displayed wide spectral bands within the range of 3374–3419 cm^{-1}, which have been attributed to the stretching vibrations of υ(OH) for the coordinated and/or hydrated water molecules of ruthenium complexes. Furthermore, the infrared spectra of complexes exhibited characteristic in-plane bending of the hydroxyl group, δ(OH), at around 1460 cm^{-1}, which could be attributed to the presence of water molecules associated with the reported complexes[46–48]. The medium-intensity bands detected at 1345, 1384, and 1304 cm^{-1} of the phenolic C-O stretching of ligands, exhibited shift towards higher wavenumbers, Table 2. These shifts in wavenumbers suggested the involvement of the phenolic oxygen in coordination[49]. In addition, the infrared spectra of the ligands displayed bands at 1613, 1590, and 1619 cm^{-1} due to the stretching vibrations of the C=N bonds of the azomethine groups. These observed bands underwent frequency shift to a range of 1602–1641 cm^{-1} because of their coordination with the ruthenium ions via their nitrogen atoms[50]. In addition, the appearance of two weak bands in the spectral range of 507–537 cm^{-1} and 439–468 cm^{-1}, which can be attributed to the stretching vibrations of the metal-oxygen, υ(M-O), and metal-nitrogen, υ(M-N), bonds, respectively, provided a conclusive proof of the coordination of the azomethine nitrogen and phenolic oxygen atoms to the metal ion[51].

The ^{1}H-NMR spectra of the investigated ligands (Figs. 6 and 7 S) have been studied in DMSO-*d6* at room temperature. Table 3 tabulates the chemical shifts corresponding to the various types of protons observed in the ^{1}H-NMR spectrum. The ^{1}H-NMR spectra of the **HL[1]**, **HL[2]** and **H_2L^3** ligands exhibited singlet peaks at 10.33,

Compound	UV-vis (nm, DMF)	Assignments
HL^1	286, 392	π-π*, n-π*
HL^2	272, 342	π-π*, n-π*
H_2L^3	278, 354	π-π*, n-π*
$[Ru(L^1)_2(H_2O)(Cl)]$	280, 454	π-π*, CT
$[RuL^2(H_2O)(Cl)_2]$	264, 354, 410	π-π*, n-π*, CT
$[RuL^3(H_2O)_2(Cl)].H_2O$	266, 332, 422	π-π*, n-π*, CT

Table 4. Electronic absorption transitions data for the ligands and their ruthenium complexes.

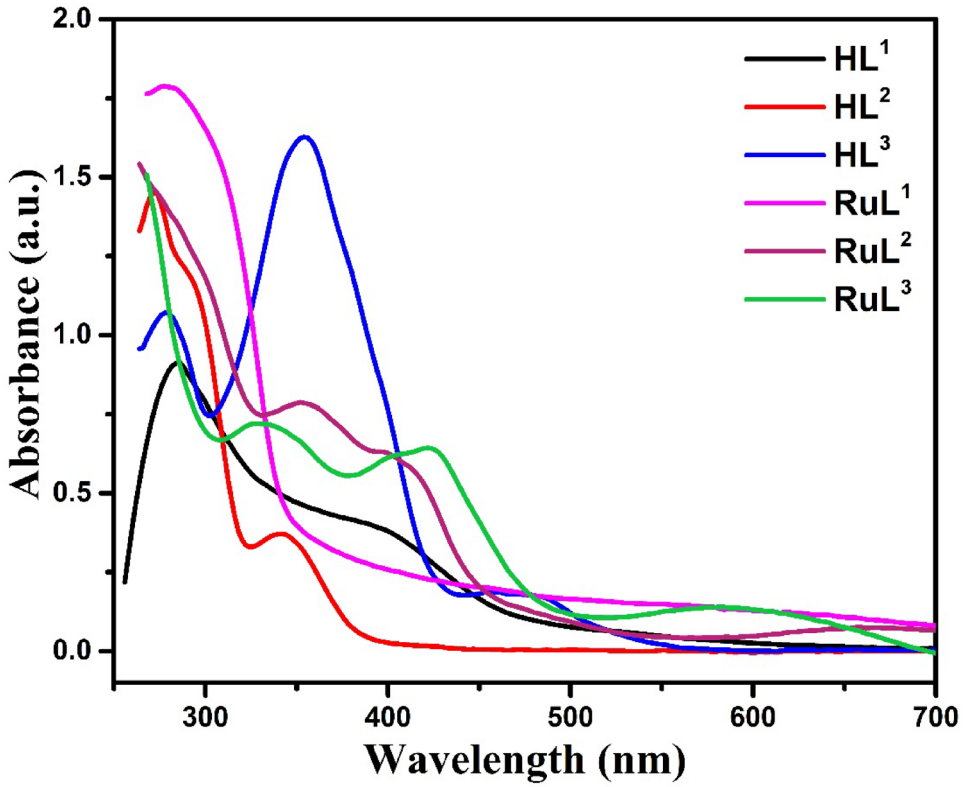

Fig. 5. Electronic absorption spectra of ligands and their complexes.

10.26 and 10.25 ppm for the phenolic hydroxyl protons, respectively. In addition, the protons of the azomethine groups displayed singlet peaks at 8.53, and 10.21 and 9.42 ppm. Further, the ^{1}H-NMR spectra of the ligands displayed multiple peaks due to the aromatic protons (Table 3). Identification of the ($-OCH_3$) moieties of $\mathbf{HL^2}$ and $\mathbf{H_2L^3}$ were also supported from their ^{1}H-NMR spectra.

Electronic absorption studies

The electronic absorption spectra of the reported compounds were performed in DMF at ambient temperature, Table 4; Fig. 5. The absorption spectra of the ligands displayed two high intensity and were assigned to π–π* and n–π* transitions due to electrons on benzene rings and the C = N chromophore[52]. These bands were shifted in the spectra of complexes due to coordination of nitrogen pair of electrons to the metal and hence the bonding of azomethine to the metal ions. In addition, the complexes exhibited a weak broad band in the 400–500 nm range due to ligand-to-metal charge transfer (LMCT) transitions[53,54].

Thermal analysis

The thermal analysis approach is widely regarded as a highly effective method for determining the quantity and nature of water molecules associated with metal complexes. This is achieved by evaluating the percentage of mass loss through the heating process[55]. Therefore, the thermogravimetric analysis of the three ruthenium complexes was carried out in air, reaching temperatures up to 1000 °C with a heating rate of 10 °C per minute, Figs. (10–12 S). The results obtained demonstrated that the complexes under investigation exhibited significant thermal stability. The decomposition processes of these complexes occurred in two or three distinct steps, involving the

partial detachment of the hydrated and coordinated water along with the organic ligands' moieties (Table 5). Ultimately, the decomposition ended with the formation of metallic oxide and carbide residues.

The breakdown action of **RuL[1]** complex comprised two distinct decomposition stages. The initial stage took place within the temperature range of 36–418 °C and was associated with the release of coordinated H_2O and C_3H_9NOCl fragments. During the ensuing second stage, which occurred within the temperature range of 419–755 °C, the liberation of $C_5H_5N_5O$ fragments was observed, resulting in the formation of metallic ruthenium residue. On the other hand, three distinct phases were involved in the decomposition of the **RuL[2]** complex. The first phase involved the release of coordinated water (H_2O) and $C_2H_2N_2$ fragments, and took place between 36 and 232 °C. The second stage was defined by the release of $C_6H_{10}N$ moieties and occurred within the 233–388 °C range. The third instance of mass loss occurring within the temperature range of 389 to 589 °C was attributed to the liberation of 2HCl, leading to the formation of metallic residue. Ultimately, the **RuL[3]** complex experienced disintegration via a sequence of three discernible decomposition phases. The first phase, occurring between temperatures of 33–140 °C, involved the release of a water molecule in its hydrated form. The second phase (141–390 °C) was characterized by the release of CH_2NCl species and two coordinated H_2O. The third decomposition stage that took place in the temperature range of 391 to 550 °C was ascribed to the dissociation of C_7H_6N, leading to the formation of metallic ruthenium residue.

Molecular orbital calculations

The energy optimized geometry, structural parameters, and the global reactivity parameters of the three ruthenium complexes were performed using DFT/B3LYP method. The energetically stable structures of the complexes were determined by focusing on the ruthenium core and the spatial arrangement of coordinated HC = N, OH, and water molecules. The energetically optimized geometries of the ruthenium complexes, **RuL[1]**, **RuL[2]** and **RuL[3]**, were investigated and the calculated energy minimized structures, numbering systems, lengths of bonds, and angle values around the metal are shown in Fig. 6. All the complexes illustrated energetically stable patterns with distorted octahedral arrangement and minimization energy = 247.22, 127.34 and 184.95 kcal/mol for **RuL[1]**, **RuL[2]** and **RuL[3]**, respectively. The distortion of the octahedral structures is clearly noticed from the deviation of the bond angles and bond lengths from the regular octahedron arrangement. It is worth mentioning that the N-Ru-N, N-Ru-O and O-Ru-O angles in the three complexes are wider than the other bond angles in the coordination core (Fig. 6). This could be probably due to the repulsive forces between the electronegative donor atoms. Interestingly, the **RuL[2]** complex illustrated intramolecular hydrogen bond between one of the pyrazine nitrogen and proton of the adjacent coordinated water (H…*N* = 1.46 Å. It is noteworthy that the remaining bond lengths and angles exhibited values consistent with those typically observed in related structures[45,56,57].

The highest occupied molecular orbital (*HOMO*) and the lowest unoccupied molecular orbital (*LUMO*) in the molecular orbital diagram of a molecule are very useful expressions for the optical, electric properties and charge transfer (CT) transitions of that molecule[44,58]. Figure 7 represents the *HOMO* and *LUMO* orbitals and energies of the investigated ruthenium complexes as well as the energy gap (ΔE) values. The reactivity descriptors of the complexes, such as E_{HOMO}, E_{LUMO}, energy gap (ΔE), chemical hardness (η), chemical potential (V), electron affinity (EA), ionization potential (IP), electronegativity (χ), electrophilicity index (ω) and chemical softness (S) were determined by the DFT calculation and are tabulated in Table 6. The donation characteristics within the molecule as represented by E_{HOMO} values are almost equal for the three complexes, while the accepting properties reflected by the E_{LUMO} values are diverse. The **RuL[1]** complex showed the highest negative E_{LUMO} value and consequently the lowest energy gap (ΔE = 1.72 eV), which might explore its increased degree of reactivity and would have facile charge transfer and polarization within the molecule. Variations in electronegativity (χ) are related to differences in electrostatic chemical potentials. The values of χ for the investigated complexes have the order **RuL[1]** > **RuL[2]** > **RuL[3]**. The capacity for charge transfer within these derivatives is reflected in their chemical hardness (η) parameters. Notably, the order of chemical hardness is inversely related to the order of electronegativity. Furthermore, the electrophilicity index (ω) of the complexes has a reverse order to their chemical softness (S) values that reflected to their biological properties.

Compound	Empirical formula	Temp. range (°C)	Mass loss (%)		Assignment
			Found	Calc.	
RuL[1]	$C_{24}H_{16}N_6O_7Cl_3Ru$	36–418	31.49	32.71	$H_2O_{(coordinated)} + C_3H_9NO_3Cl_3$
		419–755	20.51	21.33	$C_5H_5N_5O$
RuL[2]	$C_{14}H_{18}N_3O_4Cl_2Ru$	36–232	18.34	19.38	$2H_2O_{(coordinated)} + C_2H_2N_2$
		233–388	21.19	20.68	$C_6H_{10}N$
		389–589	16.46	15.72	2HCl
RuL[3]	$C_{13}H_{16}N_2O_6ClRu$	33–140	3.15	4.16	$H_2O_{(hydrated)}$
		141–390	21.79	22.99	$CH_2NCl + 2\ H_2O_{(coordinated)}$
		391–550	25.45	24.03	C_7H_6N

Table 5. Thermogravimetric data of the studied ruthenium complexes (**1–3**).

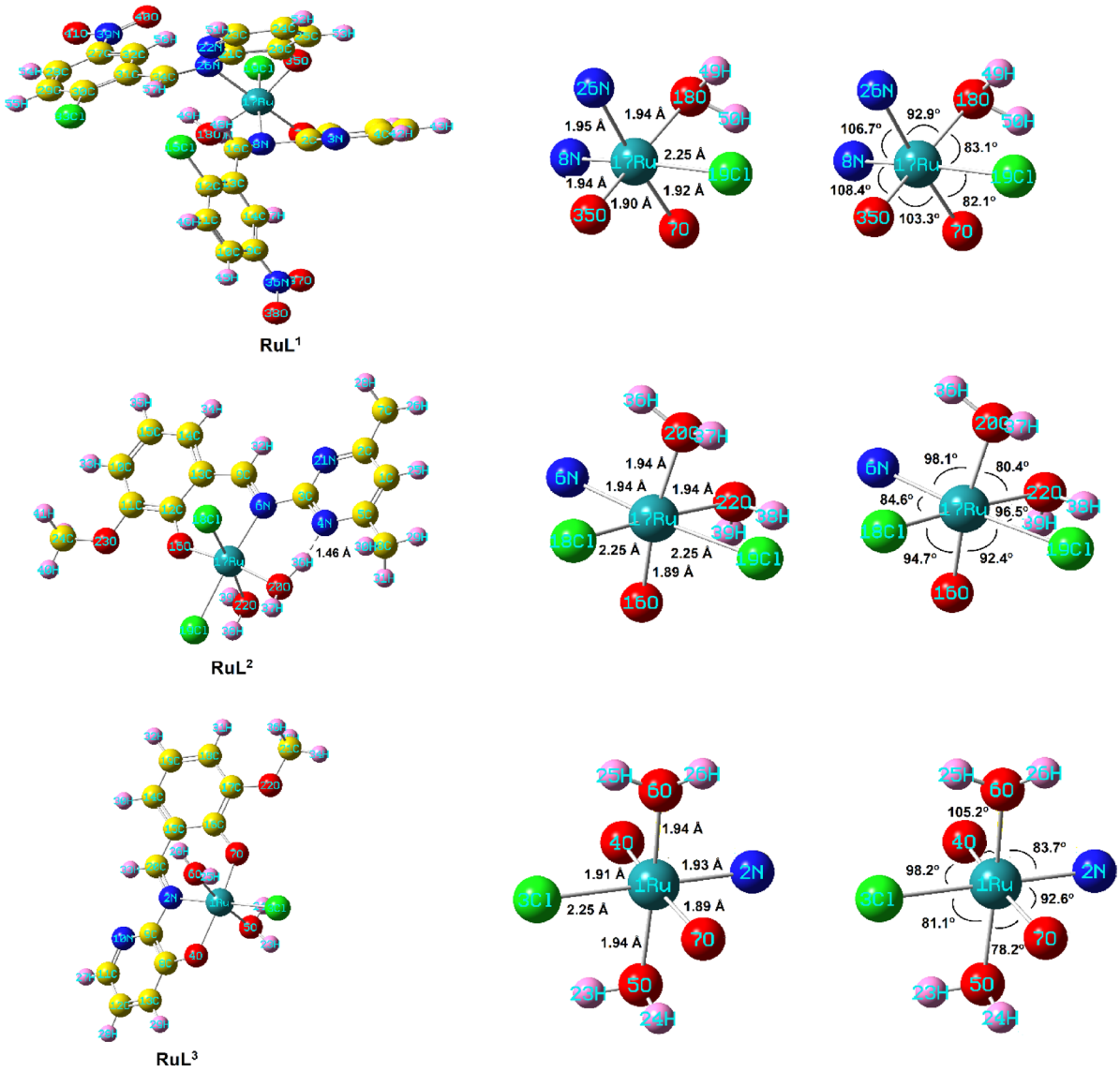

Fig. 6. Energy optimized geometries of the studied ruthenium complexes.

Biological studies

In vitro antimicrobial activities of the reported complexes

The biological functions of metallic complexes are determined by a combination of several factors. These include the chelate effect exhibited by Schiff base ligands, the specific characteristics of the donor atoms involved, the overall charge carried by the complex, the identity of the metal ion, the nature of the counter ions that neutralize the complex, and the geometric arrangement of the complex[59,60]. The process of chelation leads to a decrease in the polarity of the metal ion. This reduction occurs through a mechanism involving the partial sharing of the positive charge of the metal ion with the donor groups of the ligand. Additionally, the delocalization of π-electrons across the entire chelate ring system may further contribute to this reduction in polarity[61,62]. Hence, these constituents enhance the lipophilic nature of the metal atom core, thereby augmenting the hydrophobicity and lipo-solubility of the compound. This enables the compound to effectively interact with or traverse the lipid bilayers of the microorganism membrane. Consequently, the studied antimicrobial activity of the chemicals is enhanced due to the increased rate of absorption or entrance. Because of the ability of numerous pathogenic microbes to acquire antibiotic resistance through biochemical and morphological changes, we deemed it was necessary to investigate the antimicrobial properties of the reported ruthenium complexes as novel potential antibiotic agents.

The ruthenium complexes were evaluated for their inhibitory impacts on the growth of the G^+ bacteria *Micrococcus luteus* and the two G^- bacteria *Escherichia coli* and *Serratia marcescens* as well as the three fungi *Aspergillus flavus*, *Geotrichum candidum* and *Fusarium oxysporum*. The antibacterial and antifungal activities of the complexes are represented graphically in Figs. 8 and 9. The antimicrobial efficacy of the compounds were evaluated using two different doses (15 and 30 mg/mL). The inhibitory potencies were remarkably increased

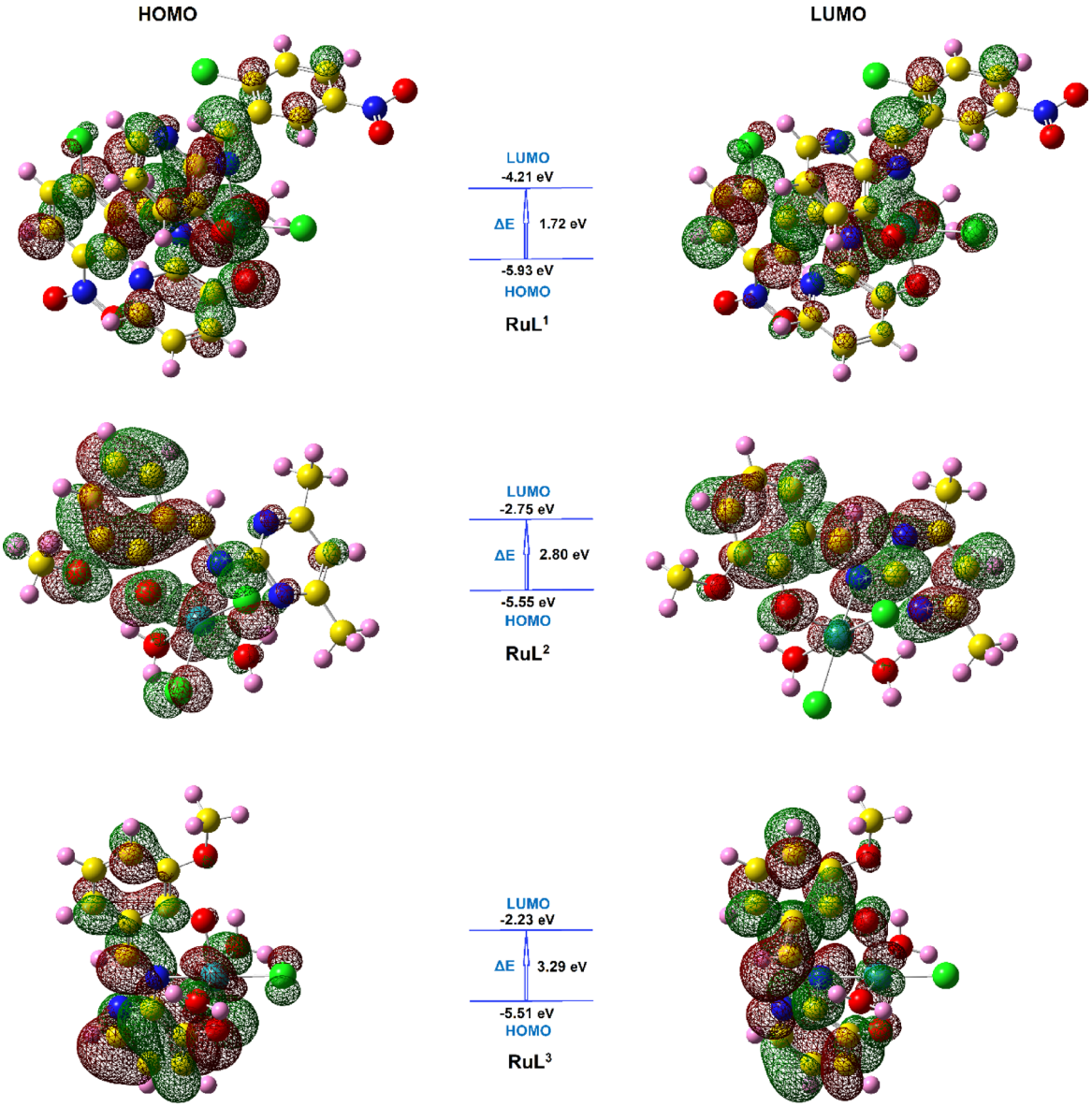

Fig. 7. The frontier *HOMO* and *LUMO* orbitals and their energy values.

Reactivity descriptor	RuL^1	RuL^2	RuL^3
Total energy (au)	−1917.40	−1133.26	−1098.23
DM (Debye)	9.37	11.26	5.32
HOMO (eV)	−5.93	−5.55	−5.51
LUMO (eV)	−4.21	−2.75	−2.23
ΔE (eV)	1.72	2.80	3.29
X (eV)	5.07	4.15	3.87
V (eV)	−5.07	−4.15	−3.87
EA (eV)	4.21	2.75	2.23
IP (eV)	5.93	5.55	5.51
η (eV)	0.86	1.40	1.64
S (eV)	0.43	0.70	0.82
ω (eV)	14.96	6.14	4.56

Table 6. The global chemical reactivity descriptors for the ruthenium complexes.

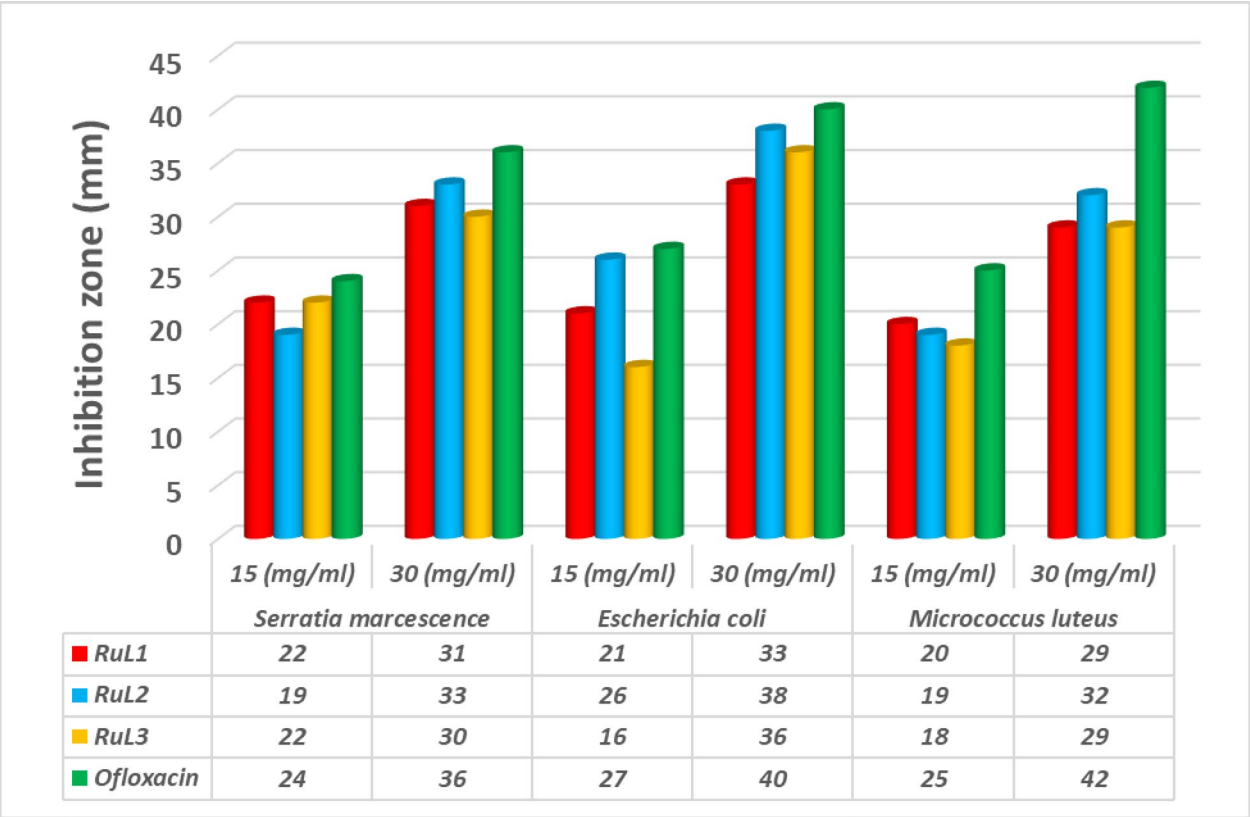

	15 (mg/ml)	30 (mg/ml)	15 (mg/ml)	30 (mg/ml)	15 (mg/ml)	30 (mg/ml)
	Serratia marcescence		Escherichia coli		Micrococcus luteus	
RuL1	22	31	21	33	20	29
RuL2	19	33	26	38	19	32
RuL3	22	30	16	36	18	29
Ofloxacin	24	36	27	40	25	42

Fig. 8. The inhibitory potency of the ruthenium complexes against the tested bacteria.

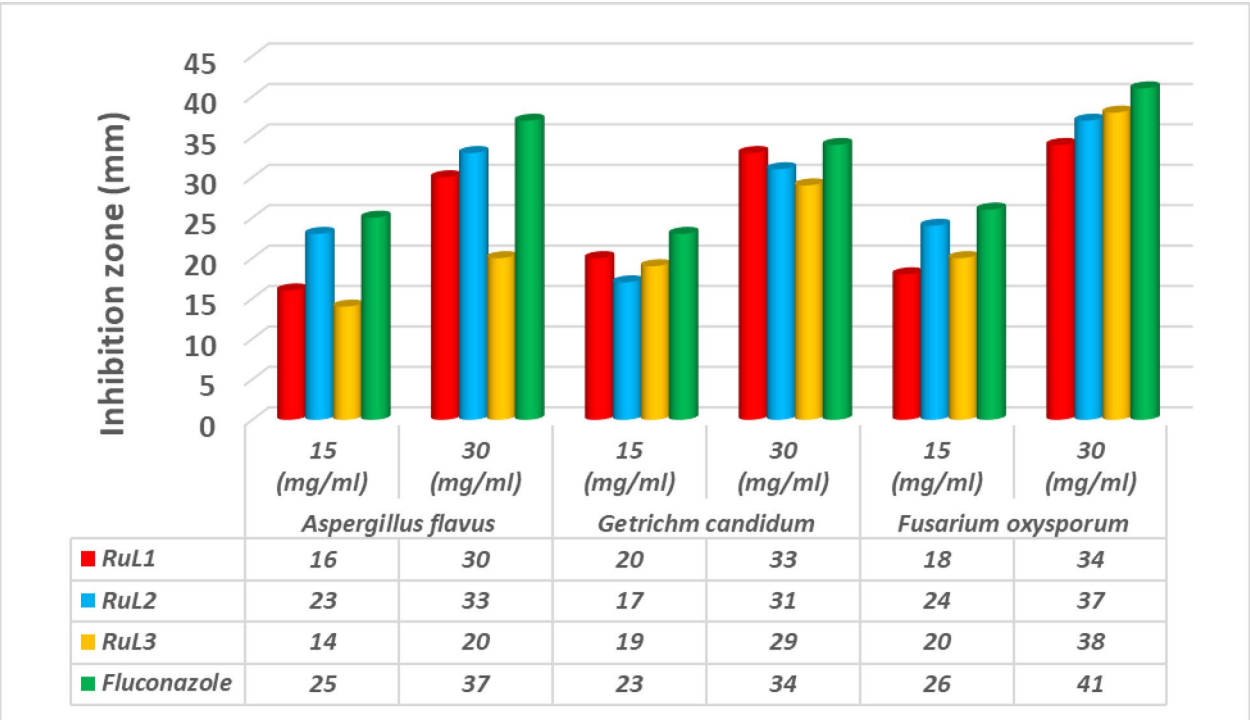

	15 (mg/ml)	30 (mg/ml)	15 (mg/ml)	30 (mg/ml)	15 (mg/ml)	30 (mg/ml)
	Aspergillus flavus		Getrichm candidum		Fusarium oxysporum	
RuL1	16	30	20	33	18	34
RuL2	23	33	17	31	24	37
RuL3	14	20	19	29	20	38
Fluconazole	25	37	23	34	26	41

Fig. 9. The inhibitory potency of the complexes against the tested fungi.

by increasing the concentrations of the compounds investigated. The results indicated that the Ru complexes exhibited rather high activities against the tested bacterial or fungal strains, and they were comparable to those of the standards. The order of the bactericidal activity against the bacteria varied upon changing the concentration of the tested compound. Thus, at the low concentration (15 mg/mL), the activity order against the *M. luteus* bacteria was **RuL^1** > **RuL^2** > **RuL^3**, for the *E. Coli* bacteria, the order of activity was **RuL^2** > **RuL^1** > **RuL^3**, whereas the inhibition effect of the compounds on the *S. marcescens* bacteria was almost equal. On the other hand, at a concentration of 30 mg/mL, the tested compounds demonstrated good antifungal activity, comparatively slightly less than the Fluconazole standard. The fungicidal activity against *A. flavus* followed the order: **RuL^2** > **RuL^1** > **RuL^3**, whereas versus *G. candidum*, the order of activity was **RuL^1** > **RuL^2** > **RuL^3**. For *F. oxysporum*, the fungicidal activity of the complexes had the order: **RuL^2** ≈ **RuL^3** > **RuL^1**. The mechanism of efficacy of the tested compounds on the tested microbes could be due to the permeability of the complexes through the microbial cells or alterations in microbial ribosomes[63]. Furthermore, the polarity of the metal was diminished through chelation due to the involvement of the partial exchange of positively charged metal ions with the donor groups found in the overlapping ligand orbitals. Therefore, it could facilitate the delocalization of the π-electrons across the entire chelate ring, and hence enhance the ability of the complex to penetrate lipid membranes[64]. Consequently, the cell respiration might be disrupted by the complex causing the prevention of the protein synthesis, which limited the organism growth[65,66].

In vitro cytotoxicity studies

The in vitro cell viability of the HCT-116, MCF-7, and HEPG2 cancer cell lines was assessed by the reported ruthenium complexes. The chemotherapy medication Vinblastine was employed as a reference drug. The assay revealed that the examined complexes have high cytotoxic activities towards the tested cell lines. Figure 10 illustrated the IC_{50} values (concentration of a drug or inhibitor required to inhibit a biological process by 50%) for the complexes. According to the findings, the **RuL^2** complex showed the lowest IC_{50} value (4.97 µg/mL) versus the HCT-116 cell line, which is very close to that of the reference drug. The order of cytotoxic activity was: **RuL^2** > **RuL^3** > **RuL^1**. On the other hand, the **RuL^1** and **RuL^2** complexes demonstrated the most pronounced cytotoxic effects against the HEPG2 cell line, which were also close to the value of Vinblastine reference drug. Several biological factors could explain the enhanced response of HepG2 cells to **RuL^1 and RuL^2**. HepG2 cells may express higher levels of liver-specific receptors or transporters, such as organic anion-transporting polypeptides (OATPs), which could facilitate the increased uptake of the ruthenium complexes[67]. Additionally, liver metabolism may contribute to higher intracellular accumulation, as HepG2 cells possess elevated levels of metabolic enzymes involved in drug uptake and transformation. Differences in cellular pathways, such as redox potential, could also favor the activation of these complexes, enhancing their cytotoxic effects[68]. Furthermore,

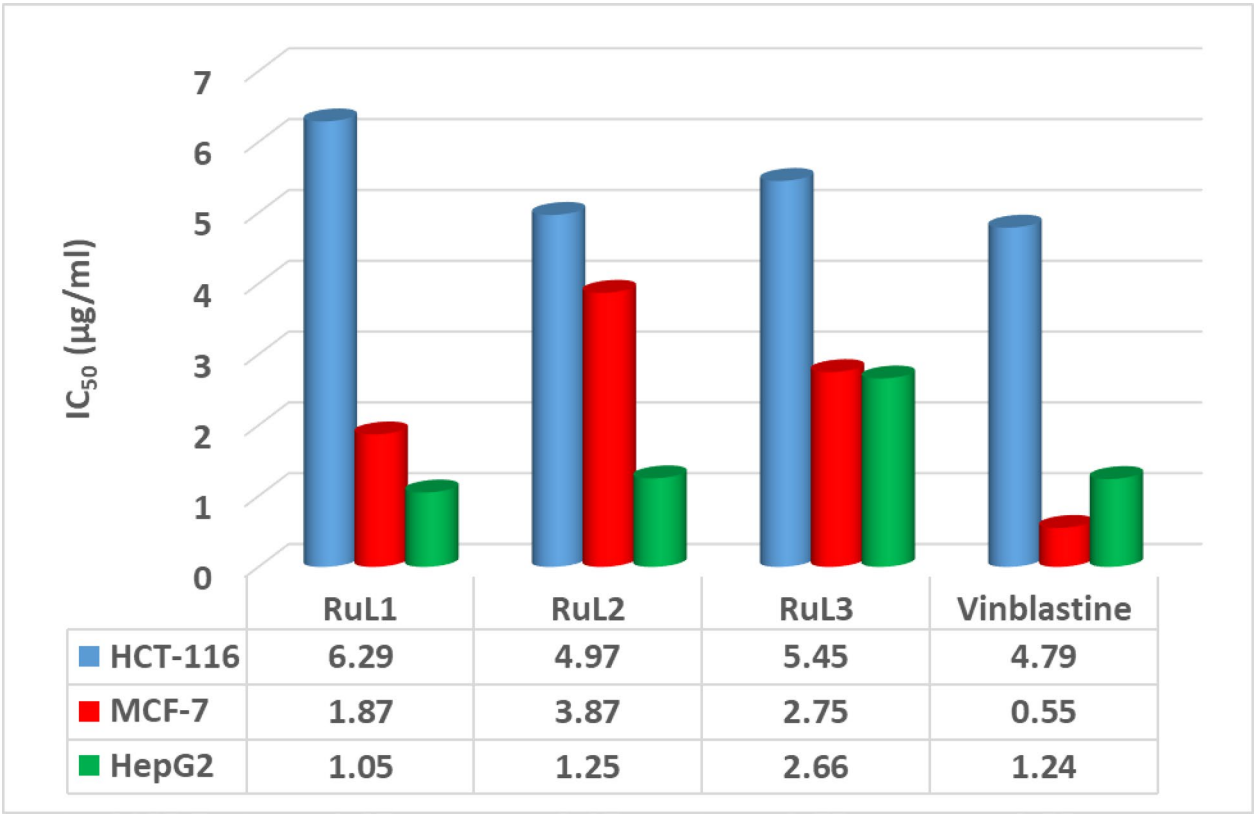

	RuL1	RuL2	RuL3	Vinblastine
HCT-116	6.29	4.97	5.45	4.79
MCF-7	1.87	3.87	2.75	0.55
HepG2	1.05	1.25	2.66	1.24

Fig. 10. The cytotoxic activity (IC_{50}) of the investigated complexes against the HCT-116, MCF-7, and HEPG2 cell lines.

the introduction of chloro and nitro groups could increase the lipophilicity of the complexes, promoting better membrane penetration and more efficient cellular uptake, while also influencing their interaction with key cellular receptors and pathways, such as redox regulation and DNA damage recognition, thereby contributing to selective toxicity in liver cancer cells[69]. Many investigations of ruthenium complexes, especially those of bioactive pyrimidine ligands, explored their privileged activity against HEPG2 cell line. A specific ruthenium(III) Schiff base complex, containing 2-chloro-5-nitrophenyl and 4,6-dimethylpyrimidinyl groups, has demonstrated potent anticancer activity against the HEPG2 cell line, with an IC50 of 29 μM. This complex triggers cell death (apoptosis) and halts cell division in the S phase, suggesting its potential as a therapeutic drug, as supported by biological and molecular docking studies[30]. These findings are particularly encouraging when compared to the cytotoxic activity of the standard medications. The sequence of activities against HEPG2 cell line was determined to be **RuL^1 > RuL^2 > RuL^3**. The IC50 data (μg/ml) for the studied complexes, relative to the Vinblastine standard, are illustrated in Fig. 10.

Molecular docking

In silico molecular docking is a widely used computational technique to simulate the binding interactions between small, synthesized molecules and biological macromolecules (receptors) such as proteins or DNA. These molecular interactions play crucial roles in numerous biological processes[70,71]. Understanding the structures and binding sites of biologically active receptors is crucial for elucidating the diverse binding modes and affinities between interacting molecules. Bioactive Schiff base derivatives and their transition metal complexes have emerged as promising pharmacophores with significant applications in medicine and pharmaceutical chemistry[72]. Extensive molecular docking studies were conducted to investigate the interactions of the bioactive Schiff base metal complexes with a wide range of macromolecular targets[71]. Therefore, the reported ruthenium complexes were subjected to molecular docking determination to realize the types of compound-target interactions and to recognize the potential binding modes and energy. The methodology of molecular docking was validated to guarantee that the procedures and input parameters were reliable and generate accurate prediction for the guest-host interactions. So, the validation operation was constructed on many factors like RMSD (root mean square deviation) value, scoring function values and the amounts and types of binding interactions. The RMSD values are considered the important key parameters for concluding the accuracy of the docking procedure. The RMSD value estimates the average space between the atomic positions of the docked guest and its original conformation. The method is considered optimally accepted with high precision when the RMSD value is less than 2 Å. However, the method is still acceptable and reasonably reliable if the RMSD value is between 2 and 3 Å[73]. Penicillin-binding protein 3 from *Escherichia coli* and B-DNA were selected as macromolecular biological targets for molecular docking studies. This selection aims to correlate the computational data obtained from docking analysis with the experimental results from antibacterial and cytotoxicity assays. Values of binding score (S), hydrophobic, and different H-bonding interactions were checked to evaluate the different conformations of the docked species with the biological targets. The high negative docking scores presented in Table 7 indicate strong binding affinities of the ruthenium complexes to the investigated targets, suggesting their potential efficacy. Figures 11 and 12 visually depict the various docking interactions, while Table 7 provides a comprehensive summary of the calculated docking results, including score function values, root-mean-square deviation (RMSD) values, and the types and energies of bonding interactions.

The amino acid fragments lysine (Lys), glutamic acid (Glu), glycine (Gly), aspartic Acid (Asp), threonine (Thr), asparagine (Asn), valine (Val), arginine (Arg), tyrosine (Tyr), alanine (Ala), and proline (Pro) were

Compound		RMSD value* (Å)	S (kcal/mol)	Ligand-receptor	Interaction type	Interaction distance (Å)	E (kcal/mol)
RuL^1	1BNA	1.71	−3.33	N11-OP1 (DG 10 A) N38-OP1 (DT 19B)	Ionic Ionic	3.60 3.93	−1.5 −0.7
	4BJP	0.99	−3.86	O25-OE1 (GLU 340 A) CL28-O (GLU 340 A) O54-NZ (LYS 499 A) O25-OE1 (GLU 340 A)	H-donor H-donor H-acceptor Ionic	2.86 3.01 3.19 2.86	−8.7 −0.4 −2.5 −5.5
RuL^2	1BNA	2.64	−4.30	O35-OP1 (DC 21B) O31-OP1 (DC 21B) O35-OP1 (DC 21B)	H-donor Ionic Ionic	2.72 3.03 2.72	−22.5 −4.3 −6.7
	4BJP	2.06	−3.85	O31-OE2 (GLU 340 A) O35-OE1 (GLU 340 A) O35-OE2 (GLU 340 A) N7-OE2 (GLU 340 A) O31-OE2 (GLU 340 A) O35-OE1 (GLU 340 A) O35-OE2 (GLU 340 A)	H-donor H-donor H-donor Ionic Ionic Ionic Ionic	2.71 3.21 2.91 3.10 2.71 3.21 2.91	−25.2 −8.7 −1.7 −3.8 −6.7 −3.2 −5.1
RuL^3	1BNA	1.67	−5.18	O8-OP1 (DG 10 A) N2-OP1 (DG 10 A) O8-OP1 (DG 10 A) 6-ring-C5' (DG 10 A)	H-donor Ionic Ionic π-H	2.67 3.50 2.67 3.48	−19.8 −1.9 −7.1 −0.6
	4BJP	1.05	−3.84	O5-OE1 (GLU 292 A) O8-OE1 (GLU 292 A) O5-OE1 (GLU 292 A) O8-OE1 (GLU 292 A) O8-OE2 (GLU 292 A)	H-donor H-donor Ionic Ionic Ionic	2.92 2.91 2.92 2.91 3.81	−17.2 −21.1 −5.1 −5.1 −0.9

Table 7. The molecular Docking interaction data for the ruthenium complexes.

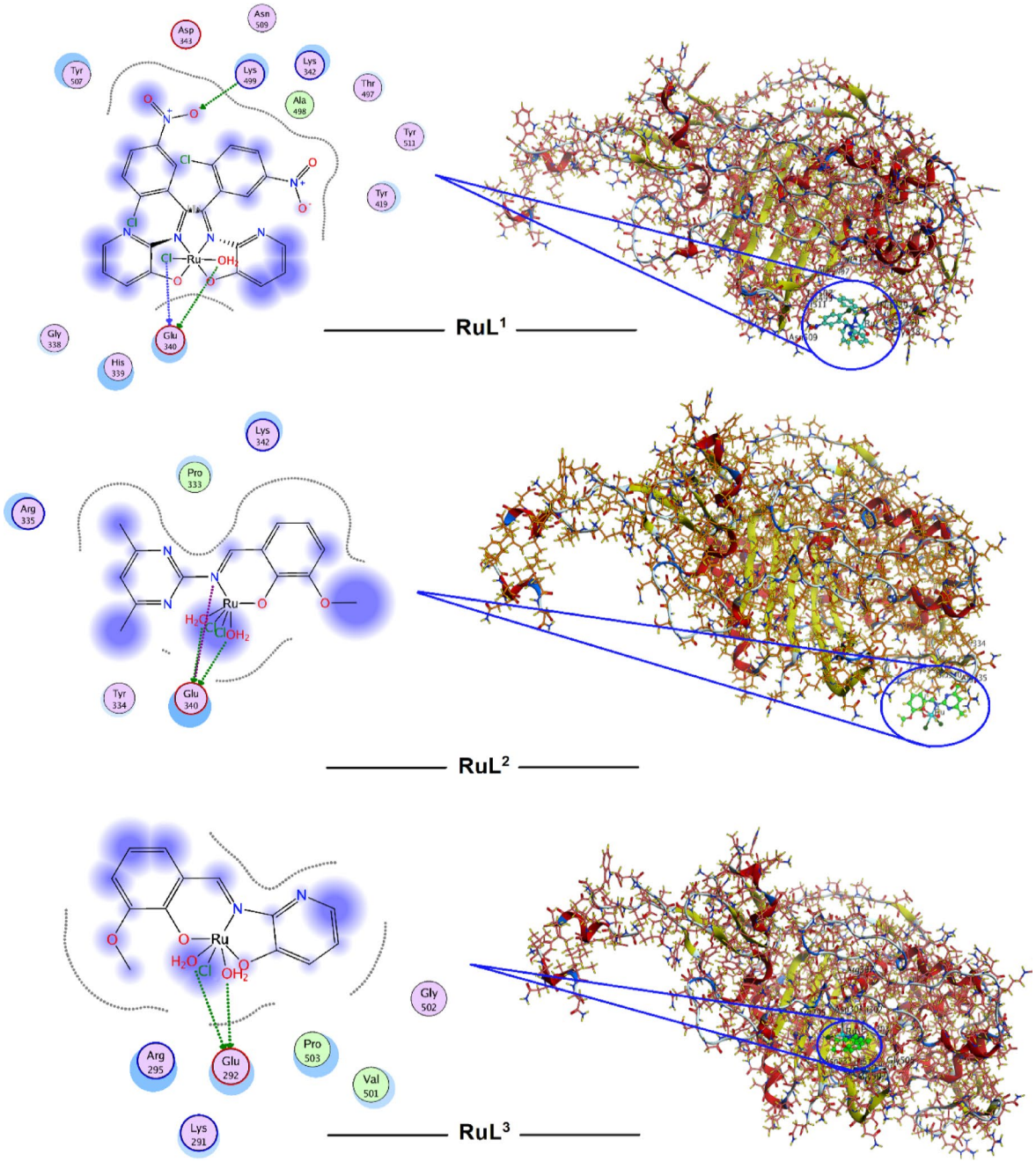

Fig. 11. *E. Coli* (PDB ID: 4BJP) docking interactions with investigated Ru complexes.

the most interacted residues of the target 4BJP (*E coli*) with the docked ruthenium complexes (Fig. 11). The interactions varied between polar-sidechain acceptors (Tyr, Asn, Thr and Gly), acidic-sidechain donors (Glu and Asp), basic-backbone acceptors (Lys and Arg), and backbone donors (Ala, Pro and Val) along with ionic interactions (Table 7). All the three ruthenium complexes displayed almost the same binding affinity towards 4BJP target (S = ≈ -3.8 kcal/mole). Such behavior is correlated with the experimental findings as the complexes exhibited comparable activity towards *E coli* bacteria especially at 30 mg/ml concentration (Fig. 8).

The three ruthenium complexes interacted with DG, DT, DC, and DA nucleotide residues of the DNA (1BNA) receptor via either backbone donor or ionic-metal complex interactions (Table 7; Fig. 12). According to the score function values, the molecular binding abilities were ordered as: **RuL^3** > **RuL^2** > **RuL^1**. While the observed order of cytotoxic effects against the tested cell lines did not perfectly align with the order suggested by the docking studies, the combined results from both experimental and computational analyses strongly suggest that the reported ruthenium complexes possess significant potential as bioactive agents and warrant further investigation as potential drug candidates.

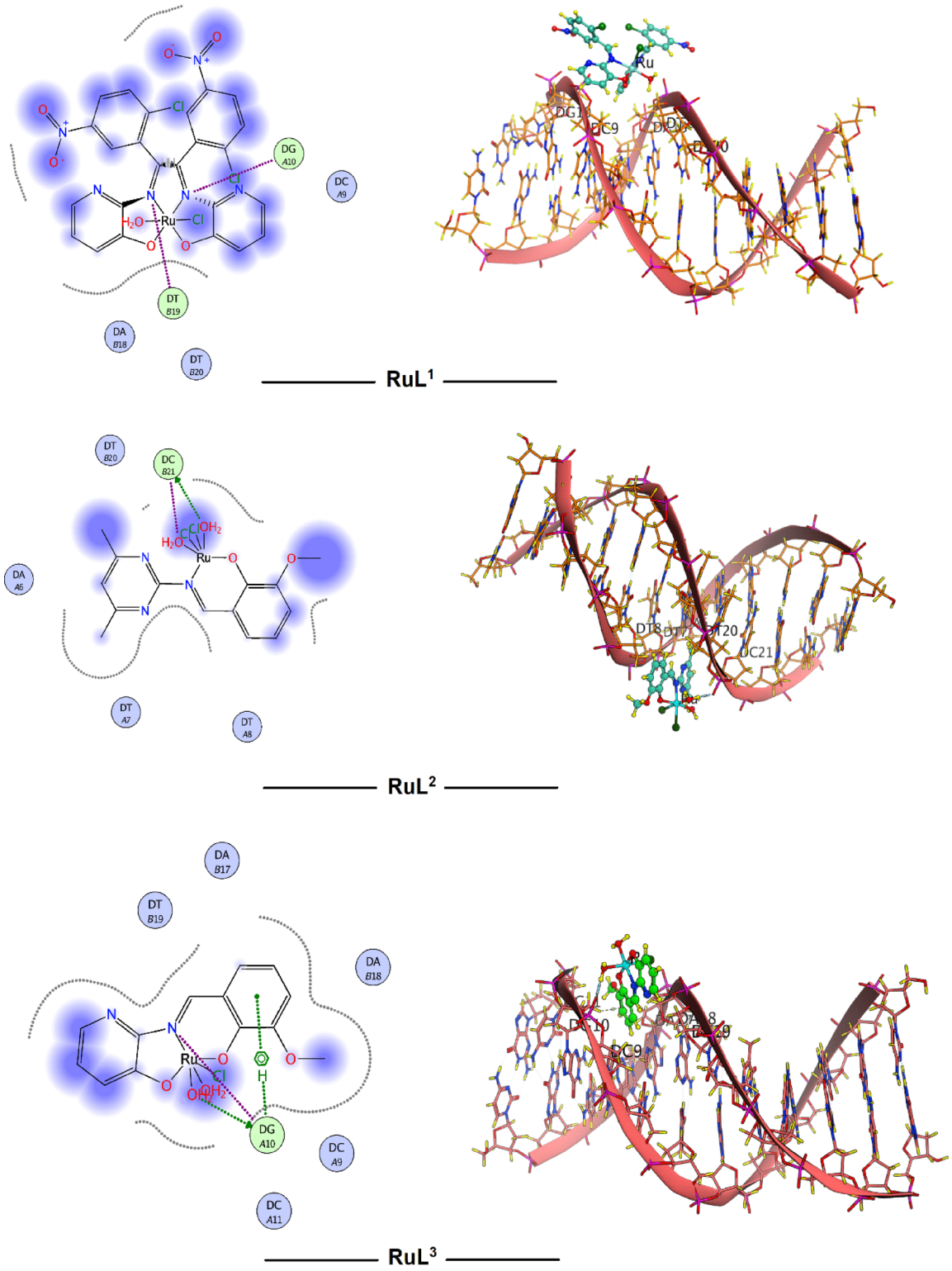

Fig. 12. B-DNA (PDB ID: 1BNA) docking interactions with investigated Ru complexes.

Conclusions

Novel mononuclear Ru(III) complexes with three diverse Schiff base ligands were successfully synthesized, exhibiting notable correlations between their structure and biological activity. Analysis of the molecular geometries and global reactivity parameters of the complexes by DFT method exhibited their unique structural arrangements and reactivity. Notably, the ruthenium complexes displayed antibacterial and antifungal activities, on par with established standard compounds. The order of bactericidal activity varied depending on the

concentration of the tested compounds, highlighting their potential for selective and concentration-dependent antimicrobial applications. The biological and molecular docking investigations revealed their potential for use in various applications, including antibiotic and anticancer treatments. The integration of theoretical and experimental findings provided deeper insights into the possible applications of these complexes as bioactive agents, indicating their potential as therapeutic drugs. So, further in vivo studies are eagerly required to explore the potent capabilities of these complexes to be used as effective reagents in the pharmacology fields. Future research endeavors encompass the synthesis and characterization of structurally analogous Ru(III)-Schiff base complexes featuring modified ligands with the objective of assessing potential enhancements in their biological activities. Additionally, exploring structural modifications could enhance selectivity and potency, paving the way for the development of targeted metal-based drugs.

Data availability

All data generated or analyzed during this study are included in this published article and its supplementary information files.

Received: 16 November 2024; Accepted: 19 May 2025
Published online: 27 May 2025

References

1. More, M., Joshi, P., Mishra, Y. & Khanna, P. Metal complexes driven from schiff bases and semicarbazones for biomedical and allied applications: a review. *Mater. Today Chem.* **14**, 100195 (2019).
2. Kanwal, A., Parveen, B., Ashraf, R., Haider, N. & Ali, K. G. A review on synthesis and applications of some selected schiff bases with their transition metal complexes. *J. Coord. Chem.* **75**, 2533–2556 (2022).
3. Rabiee, M., Salehi, M., Kubicki, M., Khaleghian, A. & Iraji, M. Theoretical studies and evaluation of anticancer properties of two Cobalt (III) schiff base complexes derived from 3, 5-dichloro-2-hydroxybenzaldehyde and 1, 2-phenylene Diamine. *J. Mol. Struct.* **1302**, 137495 (2024).
4. Liu, X. et al. Multidentate unsymmetrically-substituted schiff bases and their metal complexes: synthesis, functional materials properties, and applications to catalysis. *Coord. Chem. Rev.* **357**, 144–172 (2018).
5. Aziz, A. A. A. & Sayed, M. A. Some novel rare Earth metal ions complexes: synthesis, characterization, luminescence and biocidal efficiency. *Anal. Biochem.* **598**, 113645 (2020).
6. Parvarinezhad, S., Salehi, M. & Kubicki, M. New dinuclear schiff base nickel complex: investigation of intermolecular interactions via theoretical calculations, molecular Docking studies and ADMET profiling approaches survey. *J. Mol. Struct.* **1326**, 141016 (2025).
7. Parvarinezhad, S., Salehi, M. & Kubicki, M. Synthesis, characterization, spectral studies and evaluation of noncovalent interactions in co-crystal of μ-oxobridged polymeric copper (II) complex derived from pyrazolone by theoretical studies. *J. Mol. Struct.* **1260**, 132780 (2022).
8. El-Sonbati, A. et al. Synthesis, characterization of schiff base metal complexes and their biological investigation. *Appl. Organomet. Chem.* **33**, e5048 (2019).
9. El-Shalakany, H. H., Ramadan, R. M. & Sayed, M. A. New bivalent metal chelates based on an NO-donor schiff base ligand: synthesis, structural characterization, DFT simulation, biological evaluation, and molecular Docking analysis. *Inorg. Chem. Commun.* **159**, 111826 (2024).
10. Abdel Aziz, A. A., Ramadan, R. M., Sidqi, M. E. & Sayed, M. A. Structural characterisation of novel mononuclear schiff base metal complexes, DFT calculations, molecular Docking studies, free radical scavenging, DNA binding evaluation and cytotoxic activity. *Appl. Organomet. Chem.* **37**, e6954 (2023).
11. Elsheemy, W. M., Abdel Aziz, A. A., Ramadan, R. M., Kozakiewicz-Piekarz, A. & Sayed, M. A. Crystal structure, Hirshfeld surface analysis, molecular modeling, electrochemical properties, and potential medicinal activity of a novel binuclear Co (II) complex. *Appl. Organometal. Chem.* e7641.
12. Parvarinezhad, S., Salehi, M., Eshaghi Malekshah, R., Kubicki, M. & Khaleghian, A. Synthesis, characterization, spectral studies two new transition metal complexes derived from pyrazolone by theoretical studies, and investigate anti-proliferative activity. *Appl. Organomet. Chem.* **36**, e6563 (2022).
13. Mukherjee, P., Drew, M. G., Gomez-Garcia, C. J. & Ghosh, A. The crucial role of polyatomic anions in molecular architecture: structural and magnetic versatility of five nickel (II) complexes derived from AN, N, O-donor schiff base ligand. *Inorg. Chem.* **48**, 5848–5860 (2009).
14. El-Ghamry, M. A., Elzawawi, F. M., Aziz, A. A. A., Nassir, K. M. & Abu-El-Wafa, S. M. New schiff base ligand and its novel cr (III), Mn (II), Co (II), Ni (II), Cu (II), Zn (II) complexes: spectral investigation, biological applications, and semiconducting properties. *Sci. Rep.* **12**, 17942 (2022).
15. Kumar, M. et al. Recent developments in the biological activities of 3d-metal complexes with salicylaldehyde-based N, O-donor schiff base ligands. *Coord. Chem. Rev.* **505**, 215663 (2024).
16. Al Zoubi, W., Al-Hamdani, A. A. S. & Kaseem, M. Synthesis and antioxidant activities of schiff bases and their complexes: a review. *Appl. Organomet. Chem.* **30**, 810–817 (2016).
17. Aziz, A. A., Aboelhasan, A. E. & Sayed, M. A. A simple fluorescent chemosensor for detection of zinc ions in some real samples and intracellular imaging in living cells. *J. Braz. Chem. Soc.* **31**, 1635–1647 (2020).
18. Roozbahani, P., Malekshah, R. E., Salehi, M., Parvarinezhad, S. & Kubicki, M. Novel dinuclear Ni (II) schiff base complexes induced noncovalent exchanges: crystal structure investigation, electrochemical assessment, Hirshfeld surface analysis and SARS-CoV-2 Docking study. *Appl. Organomet. Chem.* **37**, e7254 (2023).
19. Bhardwaj, A. et al. Unveiling the biomedical potential of thiophene-derived schiff base complexes: A comprehensive study of synthesis, spectral characterization, antimicrobial efficacy, antioxidant activity, and computational insights. *Appl. Organomet. Chem.* **38**, e7398 (2024).
20. Bagul, A. D. et al. Experimental and computational evaluation of anti-malarial and antioxidant potential of transition metal (II) complexes with tridentate schiff base derived from pyrrolopyrimidine. *Biometals* 1–25. (2024).
21. Arafath, M. A. et al. Synthesis, characterization and anticancer studies of Ni (II), Pd (II) and Pt (II) complexes with schiff base derived from N-methylhydrazinecarbothioamide and 2-hydroxy-5-methoxy-3-nitrobenzaldehyde. *J. Mol. Struct.* **1130**, 791–798 (2017).
22. Ganji, N. et al. DNA incision evaluation, binding investigation and biocidal screening of Cu (II), Ni (II) and Co (II) complexes with isoxazole schiff bases. *J. Photochem. Photobiol., B.* **175**, 132–140 (2017).
23. Gichumbi, J. M. & Friedrich, H. B. Half-sandwich complexes of platinum group metals (Ir, Rh, Ru and Os) and some recent biological and catalytic applications. *J. Organomet. Chem.* **866**, 123–143 (2018).

24. Malik, M. A. et al. Probing the antibacterial and anticancer potential of tryptamine based mixed ligand schiff base ruthenium (III) complexes. *Bioorg. Chem.* **87**, 773–782 (2019).
25. Brabec, V., Pracharova, J., Stepankova, J., Sadler, P. J. & Kasparkova, J. Photo-induced DNA cleavage and cytotoxicity of a ruthenium (II) arene anticancer complex. *J. Inorg. Biochem.* **160**, 149–155 (2016).
26. Gou, Y., Huang, G., Li, J., Yang, F. & Liang, H. Versatile delivery systems for non-platinum metal-based anticancer therapeutic agents. *Coord. Chem. Rev.* **441**, 213975 (2021).
27. Singh, A. & Barman, P. Recent advances in schiff base ruthenium metal complexes: synthesis and applications. *Top. Curr. Chem.* **379**, 1–71 (2021).
28. Alkış, M. E., Keleştemür, Ü., Alan, Y., Turan, N. & Buldurun, K. Cobalt and ruthenium complexes with pyrimidine based schiff base: synthesis, characterization, anticancer activities and electrochemotherapy efficiency. *J. Mol. Struct.* **1226**, 129402 (2021).
29. Białek, M. J. & Latos-Grażyński, L. Palladium (II), ruthenium (II), and ruthenium (III) complexes of 23-thiaazuliporphyrin: the case of coordination-induced contraction. *Inorg. Chem.* **55**, 1758–1769 (2016).
30. Noureldeen, A. F. et al. Molecular design, spectroscopic, DFT, Pharmacological, and molecular Docking studies of novel ruthenium (III)–Schiff base complex: an inhibitor of progression in HepG2 cells. *Int. J. Environ. Res. Public Health.* **19**, 13624 (2022).
31. Munteanu, A. C. & Uivarosi, V. Ruthenium complexes in the fight against pathogenic microorganisms. *Extensive Rev. Pharm.* **13**, 874 (2021).
32. Pashanova, K. I., Poddel'sky, A. I. & Piskunov, A. V. Complexes of late transition metals of the 3d row based on functionalized o-iminobenzoquinone type ligands: interrelation of molecular and electronic structure, magnetic behaviour. *Coord. Chem. Rev.* **459**, 214399 (2022).
33. Marinova, P. E. & Tamahkyarova, K. D. Synthesis, investigation, biological evaluation and application of coordination compounds—a review. (2024).
34. Akhtar, M. J., Yar, M. S., Khan, A. A., Ali, Z. & Haider, M. R. Recent advances in the synthesis and anticancer activity of some molecules other than nitrogen containing heterocyclic moeities. *Mini Rev. Med. Chem.* **17**, 1602–1632 (2017).
35. Kadhum, A. M. et al. Advancement in schiff base complexes for treatment of colon cancer. *Rev. Inorg. Chem.* (2024).
36. Parveen, S. Recent advances in anticancer ruthenium schiff base complexes. *Appl. Organomet. Chem.* **34**, e5687 (2020).
37. Chow, M. J. et al. Discovery and investigation of anticancer ruthenium–arene Schiff-base complexes via water-promoted combinatorial three-component assembly. *J. Med. Chem.* **57**, 6043–6059 (2014).
38. Međedović, M. et al. Synthesis, characterization, biomolecular interactions, molecular docking, and in vitro and in vivo anticancer activities of novel ruthenium (III) schiff base complexes. *J. Inorg. Biochem.* **248**, 112363 (2023).
39. Frisch, M. et al. *Gaussian 09 Revision A. 1, 2009* 139 (Gaussian Inc. Wallingford CT, 2009).
40. Sauvage, E. et al. Crystal structure of penicillin-binding protein 3 (PBP3) from Escherichia coli. *PloS One.* **9**, e98042 (2014).
41. DrewH.R. et al. Structure of a B-DNA Dodecamer: conformation and dynamics. *Proc. Natl. Acad. Sci.* **78**, 2179–2183 (1981).
42. Bonev, B., Hooper, J. & Parisot, J. Principles of assessing bacterial susceptibility to antibiotics using the agar diffusion method. *J. Antimicrob. Chemother.* **61**, 1295–1301 (2008).
43. Ramadan, R. M., Abo-Aly, M. M. & Lasheen, A. A. Molecular structural, vibrational assignments, electronic structure and DFT calculations, and molecular Docking of N-benzylideneaniline and N-salicylidene-o-aminoaphenol schiff bases. *Inorg. Nano Metal Chem.* 1–10. (2021).
44. Ramadan, R. M. et al. Abdel Aziz, spectroscopic, density functional theory, nonlinear optical properties and in vitro biological studies of Co (II), Ni (II), and Cu (II) complexes of Hydrazide schiff base derivatives. *Appl. Organomet. Chem.* **35**, e6246 (2021).
45. El-Medani, S. M. et al. Spectroscopic, crystal structural, theoretical and biological studies of phenylacetohydrazide schiff base derivatives and their copper complexes. *J. Mol. Struct.* **1208**, 127860 (2020).
46. El-Desouky, M., El-Bindary, A., El-Afify, M. & Hassan, N. Synthesis, characterization, theoretical calculation, DNA binding, molecular docking, anticovid-19 and anticancer chelation studies of some transition metal complexes. *Inorg. Nano-Metal Chem.* **52**, 1273–1288 (2022).
47. Amin, M. et al. Synthesis of multifunctional mesoporous geopolymer under hydrothermal curing: high mechanical resistance and efficient removal of methylene blue from aqueous medium. *Dev. Built Environ.* **18** 100460. (2024).
48. Abdel-Aziz, A. M., Ramadan, M., Mohsen, A. & Sayed, M. A. Thermal treatment of lead-rich dust to improve fresh characteristics and adsorption behavior of autoclaved geopolymer for methylene blue dye removal. *Egypt. J. Chem.* **66**, 1633–1644 (2023).
49. Mohamed, R. G. et al. Spectroscopic, DFT, biological, DNA-binding, and antioxidant studies of some metal chelates with a novel thiazole-derived schiff base. *J. Coord. Chem.* **71**, 3665–3688 (2018).
50. Ramadan, R. M., Al-Nasr, A. K. A. & Noureldeen, A. F. Synthesis, spectroscopic studies, antimicrobial activities and antitumor of a new monodentate V-shaped schiff base and its transition metal complexes. *Spectrochim. Acta Part A Mol. Biomol. Spectrosc.* **132**, 417–422 (2014).
51. Abdel Aziz, A. A., Shawky, A. & Khalil, M. M. Synthesis, structural characterization, antimicrobial, antioxidant and DNA binding studies of some novel homo-binuclear schiff base metal (II) complexes. *Appl. Organomet. Chem.* **32**, e4404 (2018).
52. Kargar, H. et al. Synthesis, crystal structure, spectral characterization, theoretical and computational studies of Ni (II), Cu (II) and Zn (II) complexes incorporating schiff base ligand derived from 4-(diethylamino) salicylaldehyde. *Inorg. Chim. Acta*. **536**, 120878 (2022).
53. Aboaly, M. M. & Khalil, M. M. Synthesis and spectroscopic study of Cu (II), Ni (II), and Co (II) complexes of the ligand salicylidene-2-amino thiophenol. *Spectrosc. Lett.* **34**, 495–504 (2001).
54. Tsai, C. N. et al. Metal-to-ligand charge-transfer emissions of ruthenium (II) Pentaammine complexes with monodentate aromatic acceptor ligands and distortion patterns of their lowest energy triplet excited States. *Inorg. Chem.* **54**, 8495–8508 (2015).
55. Mahmoud, N. F., Mahmoud, W. H. & Mohamed, G. G. Synthesis, spectral, MOE and cytotoxic studies of nano Ru (III), Pr (III) and Gd (III) metal complexes with new schiff base ligand based on dibenzoyl methane and anthranilic acid. *Appl. Organomet. Chem.* **34**, e5801 (2020).
56. Hassen, S., Chebbi, H., Zid, M. & Arfaoui, Y. Assembly and weak interactions in the crystal structure of 2-amino-4-(3-bromophenyl)-1, 3, 5-triazinobenzimidazolium chloride studied by X-ray diffraction, vibrational spectroscopy, Hirshfeld surface analysis and DFT calculations. *J. Mol. Struct.* **1179**, 678–684 (2019).
57. Yıldız, M. et al. Synthesis, biological activity, DNA binding and anion sensors, molecular structure and quantum chemical studies of a novel bidentate schiff base derived from 3, 5-bis (triflouromethyl) aniline and salicylaldehyde. *J. Mol. Struct.* **1094**, 148–160 (2015).
58. Shruthi, C. et al. Molecular structure, Hirshfeld surface and density functional theoretical analysis of a NLO active chalcone derivative single crystal—A quantum chemical approach. *J. Mol. Struct.* **1228**, 129739 (2021).
59. Liu, R., Cui, J., Ding, T., Liu, Y. & Liang, H. Research progress on the biological activities of metal complexes bearing polycyclic aromatic hydrazones. *Molecules* **27**, 8393 (2022).
60. Karges, J., Stokes, R. W. & Cohen, S. M. Metal complexes for therapeutic applications. *Trends Chem.* **3**, 523–534 (2021).
61. Abo-Aly, M., Salem, A., Sayed, M. & Aziz, A. A. Spectroscopic and structural studies of the schiff base 3-methoxy-N-salicylidene-o-amino phenol complexes with some transition metal ions and their antibacterial, antifungal activities. *Spectrochim. Acta Part A Mol. Biomol. Spectrosc.* **136**, 993–1000 (2015).
62. Aziz, A. A. A., Salem, A. N. M., Sayed, M. A. & Aboaly, M. M. Synthesis, structural characterization, thermal studies, catalytic efficiency and antimicrobial activity of some M (II) complexes with ONO tridentate schiff base N-salicylidene-o-aminophenol (saphH2). *J. Mol. Struct.* **1010**, 130–138 (2012).

63. Mubeen, B. et al. Nanotechnology as a novel approach in combating microbes providing an alternative to antibiotics, *Antibiotics*, **10** 1473. (2021).
64. Sayed, F. N. & Mohamed, G. G. Newly synthesized lanthanides complexes of ferrocene-based schiff base with high biological activities and improved molecular Docking data. *J. Organomet. Chem.* **977**, 122450 (2022).
65. Sharma, B. et al. Antimicrobial agents based on metal complexes: present situation and future prospects. *Int. J. Biomater.* **2022** (2022).
66. Yousef, T., El-Reash, G. A. & El-Tabai, M. Comparative studies on P-vanillin and O-vanillin of 2-hydrazinyl-2-oxo-N-phenylacetamide and their Mn (II) and Co (II) complexes. *J. Mol. Struct.* **1159**, 246–258 (2018).
67. Marin, J., Briz, O., Perez, M. J., Romero, M. R. & Monte, M. J. Hepatobiliary transporters in the Pharmacology and toxicology of anticancer drugs. *Front. Biosci. (Landmark Ed).* **14**, 4257–4280 (2009).
68. Jungwirth, U. et al. Anticancer activity of metal complexes: involvement of redox processes. *Antioxid. Redox. Signal.* 15 (2011).
69. Raimondi, M. V. et al. New synthetic nitro-pyrrolomycins as promising antibacterial and anticancer agents. *Antibiotics* **9**, 292 (2020).
70. Khan, S. U., Ahemad, N., Chuah, L. H., Naidu, R. & Htar, T. T. Illustrated step by step protocol to perform molecular docking: human Estrogen receptor complex with 4-hydroxytamoxifen as a case study. *Progress Drug Discovery Biomedical Sci.* **3**, a0000054 (2020).
71. Ramadan, R. M. & Noureldeen, A. F. *12 Molecular docking and drug design of schiff base metal complexes, structural and biological applications of schiff base metal complexes* 221 (2023).
72. Chaudhary, N. K., Guragain, B., Chaudhary, S. K. & Mishra, P. Schiff base metal complex as a potential therapeutic drug in medical science: A critical review. *Bibechana* **18**, 214–230 (2021).
73. I.V. de França, Döring, T. H., de Oliveira Neto, F. M. & Pedroso, M. J. J.W. Da Cruz júnior, Imines and their metal complexes as active drugs against Chagas disease: A review in recent years and analyses of in silico properties. *J. Mol. Struct.* 138725. (2024).

Author contributions

Ramadan M. Ramadan: Conceptualization, Visualization, Resources, Formal analysis, Software, Validation, Writing – Review & editing, Supervision. Hadeel H. El-Shalakany: Methodology, Investigation, Data curation. Mostafa A. Sayed: Conceptualization, Methodology, Investigation, Data curation, Validation, Visualization, Writing – Review & editing.

Funding

Open access funding provided by The Science, Technology & Innovation Funding Authority (STDF) in cooperation with The Egyptian Knowledge Bank (EKB).

Declarations

Competing interests

The authors declare no competing interests.

Additional information

Supplementary Information The online version contains supplementary material available at https://doi.org/10.1038/s41598-025-03147-9.

Correspondence and requests for materials should be addressed to M.A.S.

Reprints and permissions information is available at www.nature.com/reprints.

Publisher's note Springer Nature remains neutral with regard to jurisdictional claims in published maps and institutional affiliations.